Characterization of Phosphorus and Ground Granulated Blast-Furnace Slags as Low-Cost Adsorbents for Cu(II) Removal; Kinetic, Isotherm, and Thermodynamic Studies

Dizaj Khalili, Ali Akbar
Faculty of Converging Sciences and Technologies, Science and Research Branch, Islamic Azad University, Tehran, I.R. IRAN

Ghaemi, Ahad*[+]
School of Chemical Engineering, Iran University of Science and Technology, Tehran, I.R. IRAN

Yusefi, Mohammad
Faculty of Pharmaceutical Chemistry, Department of Chemistry, Tehran Medical Science Branch, Islamic Azad University, Tehran, I.R. IRAN

ABSTRACT: *Cu(II) is one of the pollutants that exist in the produced wastewater by many industries. According to the World Health Organization (WHO), its concentration should be less than 2 mg/L. In this study, Phosphorus Slag (PS) and Ground Granulated Blast-Furnace Slag (GGBFS) as industrial wastes with the properties of abundant and low cost are used to remove Cu(II). The effects of the shaker rotation rate, initial concentration of Cu(II), and amount of adsorbent on the adsorption process are investigated. The adsorption capacity was maximized at a shaking rate of 150 rpm, initial concentration of 50 mg/L, 0.2 g GGBFS per 0.03 liter, and 0.5 g PS per 0.03 liter. At various temperatures, the values of thermodynamic parameters were calculated by measuring the equilibrium data. The results showed that the adsorption process was exothermic using both GGBFS and PS adsorbents. The experimental data of Cu(II) adsorption by GGBFS and PS was fitted well by Langmuir and Freundlich isotherm models, respectively. The maximum adsorption capacity was obtained 156.30 and 151.52 mg/g for GGBFS and PS, respectively. Also, the kinetic modeling indicated that the adsorption process is achieved to the equilibrium state using both adsorbents at less than 5 min.*

KEYWORDS: *Phosphorus slag; GGBF slag, Cu(II); Low-cost adsorbent; Shaking rate.*

INTRODUCTION

The expansion of industries has increased the concerns about heavy metals in wastewater [1]. Hence, various techniques including solvent extraction, precipitation, ion-exchange methods, chemical and electrochemical

***** *To whom correspondence should be addressed.*
+ E-mail: aghaemi@iust.ac.ir
1021-9986/2021/1/1126-1136 14/$/6.04

techniques, reverse osmosis, ultrafiltration, coagulation, and flotation have been used for the removal of heavy metal ions from wastewater. However, most of these techniques are unacceptable because of their low efficiency, high cost, and inapplicability to remove a wide range of heavy metals [2-4].

Adsorption is one of the most efficient methods for water treatment applications. Various adsorbents like synthetic adsorbents [2, 5, 6], mineral adsorbents [7-11], and Nanoscale adsorbents [12-14] have been utilized to separate heavy metals from wastewater. In the meantime, low-cost adsorbents are widely implemented in scientific research if they have an acceptable adsorption capacity and high industrial potential. It usually requires a higher cost and chemical additives for the adsorbent synthesis due to the use of Nano scale and synthetic adsorbents for the removal of heavy metals. Therefore, using low-cost adsorbents with a high adsorption capacity is very attractive as the use of low-cost and available adsorbents have increased in previous research [15].

Searching for readily available and low-cost adsorbents for the elimination of heavy metal ions has become a significant issue for research in the last decade. Industrial byproducts, natural substances, and agricultural wastes have been considered adsorbents for heavy metal removal. Several researchers investigated industrial byproducts such as Lignite, Kaolinite, Lignin Diatomite, Aragonite Shells, Peat, Clay, and natural Zeolites [16]. The Ground Granulated Blast-Furnace Slag (GGBFS) and Phosphorus Slag (PS) is the low-cost adsorbent that is considered an industrial byproduct and industrial waste. In this research, these two adsorbents were used for Cu(II) adsorption from wastewater.

Cu(II) is one of the heavy metals that produces several contaminants in various industries like mining, melting, corrosion of pipes, and electroplating industries [17]. The continuous consumption of Cu(II) by humans leads to diarrhea, vomiting, abdominal pain, Wilson's disease, mucosal burning, depression, and gastrointestinal, and lung cancer. The World Health Organization (WHO) recommended that the maximum acceptable amount of Cu(II) concentration in water is 2 mg/L [18]. Therefore, it is necessary to minimize the Cu(II) concentration before releasing copper-based wastewater into the environment. Several types of research have been performed on Cu(II) adsorption by various adsorbents.

Muslim et al. [19] studied the Cu(II) adsorption process by Activated Carbon (AC) prepared from Pithecellobium Jiringa Shell (PJS) waste in batch mode adsorption experiments. Their results indicated that the Cu(II) adsorption onto the PJS-AC was non-spontaneous and exothermic chemical adsorption. *Muslim et al.* [20] optimized the adsorption of Cu(II) ions on AC using the Response Surface Methodology (RSM). The optimum adsorption capacity was achieved at the conditions of 1000 mg/L, 0.5 M, 45 °C, and 5, for the Cu(II) ion concentration, setting the activator concentration, adsorption temperature, and pH, respectively. *Alasadi et al.* [21] used nano kaolinite powder as an adsorbent for the adsorption of Cu(II), Zn(II) and Ni(II) ions. They investigated the influences of initial metal ion concentration, pH, contact time, adsorbent dose, and temperature on the adsorption performance was evaluated, and found that this adsorbent could be utilized for the adsorption of heavy metals with acceptable efficiency. *Dandil et al.* [22] employed a crosslinked chitosan/Waste Active Sludge Char (WASC) beads to separate the Cu(II) ions from an aqueous solution. Their results demonstrated that the WASC beads separated 81.7% of Cu(II) from the solution with a concentration of 300 mg/L Cu(II) ions. *Ahmad et al.* [23] proposed a new Magnetic Tubular Carbon Nanofibers (MTCFs) for the separation of Cu(II) ions from wastewater. They regenerated the MTCFs for up to six cycles with the same contact for all adsorption cycles. *Yu et al.* [24] utilized a metakaolin-based mesoporous geopolymer (GP-CTAB) for the removal of Cu(II) and Cr(VI) by a simple synthetic route using cetyltrimethylammonium bromide (CTAB) as an organic modifier. The values of 108.2 and 95.3 mg/g were obtained as the maximum theoretical adsorption capacity of GP-CTAB for Cu(II) and Cr(VI), respectively.

In the present study, three influential operating variables on Cu(II) adsorption are investigated. These variables include the rotation rate of the solution containing Cu(II), the amount of adsorbent, and the initial concentration of Cu(II). Also, the studies of the adsorption thermodynamics, and kinetic and isotherm modeling have been carried out for the adsorption process by the GGBFS and PS adsorbents.

EXPERIMENTAL SECTION

The GGBFS and PS were provided by Esfahan Steel Company in Iran. All samples were made using a standard solution of $Cu(NO_3)_2$ at a concentration of 1000 mg/L.

Table 1: The chemical composition of the PS and GGBFS.

Ingredient		CaO	SiO_2	Al_2O_3	P_2O_5	Fe_2O_3	MgO	Na_2O	K_2O	SO_3	TiO_2
Contents	GGBFS	43.1	32.46	14.3	0.02	0.61	3.94	0.24	0.33	4.45	0.55
	PS	46.45	37.92	6.97	1.79	0.62	1.20	0.38	0.68	3.99	--

Table 2: BET surface and average pore size of the GGBFS and PS.

Property	GGBFS	PS
Specific surface (m^2/g)	0.9982	0.7430
Volume of the pores (mm^3/g)	2.3	1.6
Specific weight (g/cm^3)	2.85	2.95

The $Cu(NO_3)_2.3H_2O$ salt was supplied from Germany Merck company with a purity of 99.5%. The effect of pH is examined and the maximum adsorption capacity was obtained at pH value of 5.5. So, all of the experiments were carried out at a constant pH value of 5.5 adjusted by the HNO_3 and NaOH solutions with a concentration of 1 mol/L. An atomic adsorption spectrophotometer (AA-6300) was utilized to measure the Cu(II) concentration after the completion of the adsorption process.

1 g of the adsorbents was added to 30 mL of the Cu(II) solution at room temperature (25 °C) to investigate the effects of the initial concentration of Cu(II). Then, the solution containing the adsorbent was shaken at 150 rpm for 5 min. Based on the kinetics study, it was found that the adsorption process of Cu(II) is achieved to equilibrium using PS and GGBFS in a short time of 5 min. The initial concentration of Cu(II) was considered 5, 20, 50, 100, 200, 500, and 1000 mg/L. The amount of 1 gr adsorbent was added to 30 mL Cu(II) solution with a concentration of 50 mg/L at room temperature to investigate the effects of the rotation rates of 15, 60, 105, 150, and Also, a 30 mL Cu(II) solution with a concentration of 50 mg/L was used to examine the influence of adsorbent weight at room temperature and the rotation speed of 150 rpm. For this purpose, the weight of each adsorbent was taken into consideration in the amount of 0.1, 0.2, 0.5, 1, and 2 g. It should be noted that all experiments were repeated three times and the average values of adsorption capacity were reported in this research.

THEORETICAL SECTION

There is gravity between the Cu(II) and negative heads of the polar H_2O molecules in the aqueous solution, which causes the dissolving of the Cu(II) in water presented in Eq. (1).

$$Cu^{2+} + 4H_2O \rightarrow Cu^{2+}(H_2O)_4 \quad (1)$$

Since the adsorption of metals is usually achieved through the formation of a complex at the adsorbent surface [25-27], the copper ions form a complex on the adsorbent surface and remove from the solution due to the formation of van der Waals force between the Cu(II) and adsorbents (PS or GGBFS) by adding the adsorbents to the solution. The surface complexion is shown in Eq. (2).

$$Cu^{2+}.4H_2O + PS/GGBFS \rightarrow Cu^{2+}.4H_2O.PS/GGBFS \quad (2)$$

RESULTS AND DISCUSSION

Characterization of adsorbents

The chemical composition of the adsorbents was determined using the X-ray fluorescent (XRF) analyzer (ARL-72000 S), and its results are presented in Table 1. The principal mineralogical phases identified in both adsorbents are quartz (SiO_2) and calcium oxide (CaO). With consideration of the chemical composition, these slags are almost neutral with the basicity coefficients of (K_b= (CaO + MgO) /(SiO_2 + Al_2O_3)) 0.97 and 1.06 for GGBFS and PS , respectively [28].

Table 2 presents the surface area of the adsorbents measured by the surface area analysis (ASAP 2020). According to the obtained data, the specific surface of the GGBFS is greater than the PS one.

The covalent bonds of the chemical compounds were examined for the adsorbents by the Fourier Transform InfraRed (FT-IR) spectrophotometer (FTIR-8400 S) shown in Fig. 1. As can be observed, the observed peak at a wavenumber of 2358 (1/cm) relates to a dual carbon

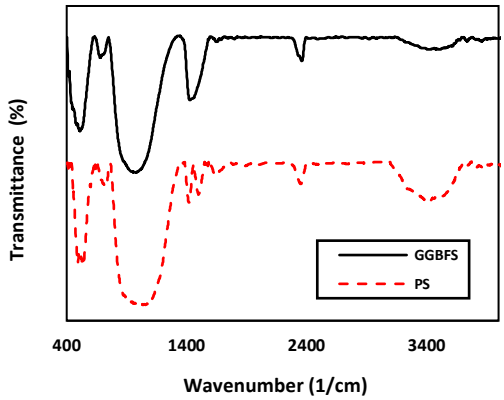

Fig. 1: The FTIR spectra of PS and GGBFS.

and oxygen bonds that indicate the adsorption of carbon dioxide presented in the air by the adsorbent. In addition, the observed peak in the range of 3100-3700 (1/cm) relates to the single bonds of hydrogen and oxygen in water vapor of air adsorbed by the adsorbent. According to Fig. 1, the GGBFS has almost been dry at the test, but PS had some moisture. The peaks in the range of 680-760 (1/cm) and 1350-1550 (1/cm) demonstrate the presence of SO_3 and P_2O_5 in the samples, respectively. The peaks in the ranges of 800-1300 (1/cm) and 400-650 (1/cm) attribute to some metal-oxygen bonds such as SiO_2, Al_2O_3, Fe_2O_3, MgO, Na_2O, K_2O, and TiO_2 [29].

Adsorption kinetics

In this work, two kinetic models were utilized to evaluate the Cu(II) kinetic adsorption; the First-order model and the second-order model. The linearized relation between adsorption capacity (q_e) and time in the first-order model is given in Eq. (3) [30].

$$\ln(q_e - q_t) = \ln q_e - k_1 t \quad (3)$$

Where q_e and q_t represent the amount of adsorbed metal at the equilibrium state and at time t, respectively. The parameter of k_1 is the constant rate of adsorption. By plotting $ln(q_e\text{-}q_t)$ versus time, a line is obtained that the value of k_1 is calculated from its slope and the value of q_e is calculated from its intercept. The differential equation of the second-order model is presented in Eq. (4) [31] which transfers to Eq. (5) by linearization. By plotting this linear relation, the values of q_e and k_2 are obtained from the slope and intercept of the plot.

$$\frac{dq}{dt} = k_2 (q_e - q_t)^2 \quad (4)$$

$$\frac{t}{q_t} = \frac{1}{k_2 q_e^2} + \frac{1}{q_e} t \quad (5)$$

The linear diagrams of the first-order model for GGBFS and PS adsorbents are illustrated in Fig. 2A. According to this figure, the first-order model cannot justify the experimental data. The linear diagrams of the second-order model for GGBFS and PS adsorbents are shown in Figs. 2B and 2C, respectively. From the obtained results, the second-order model fits well the experimental data for Cu(II) adsorption by both GGBFS and PS adsorbents. The kinetic parameters of the first-order and second-order models are also presented in Table 3. Based on the reported data, the R^2 value of 1 confirmed that the second-order model had a high precision prediction for the experimental data by these adsorbents.

Adsorption isotherms

Isotherm models express the relationship between the amount of adsorbed metal (q_e) and the amount of metal remaining in the solution (C_e) at a constant temperature after reaching equilibrium. In this research, the models of Langmuir and Freundlich are applied to study the adsorption isotherm. The linear form of the Freundlich model is presented in Eq. (6) [32] and used for multi-layers adsorption on heterogeneous surfaces [33].

$$\ln q_e = \ln k_f + n \ln C_e \quad (6)$$

The Langmuir isotherm model assumes that the adsorption process occurs homogeneously. This means that all sites have the same tendency for metal adsorption [34]. The adsorbed particles on the adsorbent surface have no migration and also are adsorbed in the one-layer form [35]. The non-linear equation of the Langmuir model is given in Eq. (7) [36].

$$q_e = \frac{q_m K_L C_e}{1 + K_L C_e} \quad (7)$$

Where K_L is the Langmuir isotherm constant, q_m is the maximum theoretical adsorption capacity and q_e is the equilibrium adsorption capacity. The results of the Langmuir isotherm are depicted in Fig. 3. As can be observed, the Langmuir isotherm can predict the experimental data

Table 3: Kinetic parameters for the sorption of Cu(II) ions by GGBFS and PS on the first order and second order kinetic models.

Kinetic equation	Parameters	Adsorbent	
		GGBFS	PS
First order	K_1 (1/min)	0.00007	0.00003
	$q_{e\,(cal.)}$ (mg/g)	146.47	145.98
	R^2	0.2634	0.2966
Second order	K_2 (g/mg. (1/min)	0.670	0.680
	$q_{e\,(cal.)}$ (mg/g)	1.4802	1.4771
	R^2	1	1
$q_{e\,(exp.)}$ (mg/g)		1.4790	1.4734

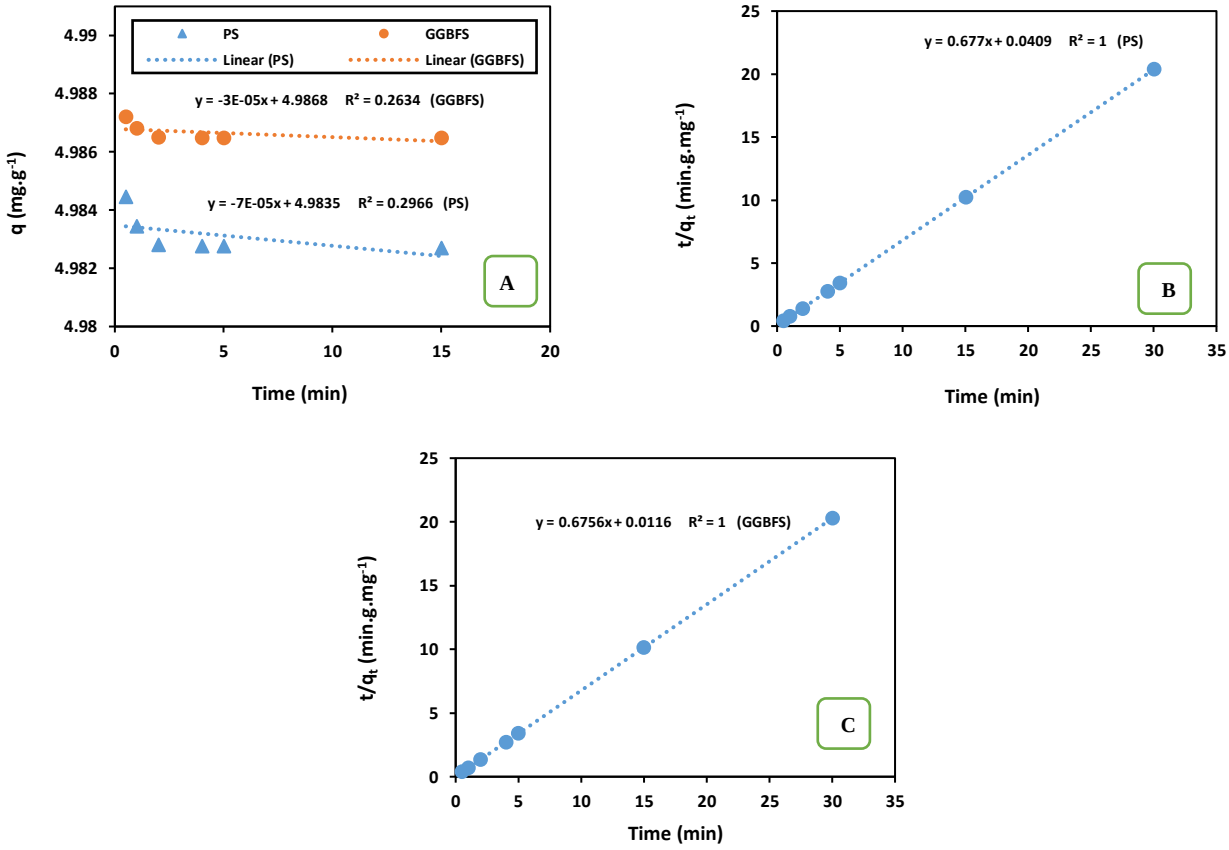

Fig. 2: Kinetic adsorption data for Cu(II) removal; (A) The linear first-order kinetic adsorption using GGBFS and PS, (B) The linear second-order kinetic adsorption using PS, and (C) The linear second-order kinetic adsorption using GGBFS.

of the Cu(II) adsorption accurately for both adsorbents. Moreover, the prediction accuracy for GGBFS is higher than PS. The parameters of the Langmuir and Freundlich isotherms are listed in Table 4. As shown, the Langmuir model is a higher accurate model than the other because its R^2 values are larger than 0.98 for both adsorbents.

Webber and *Chakkravorti* introduced a dimensionless number called the separation factor to evaluate the adsorption process in the Langmuir model that was presented in Eq. (80 [37].

$$R_L = \frac{1}{1 + K_L C_0} \tag{8}$$

Where K_L (L/mg) is the Langmuir constant and C_0 (mmol/L) is the initial concentration of Cu(II). If $R_L > 1$, the adsorption process is undesirable, $R_L = 1$ shows

Table 4: Isotherm parameters of the Langmuir and Freundlich models for the sorption of Cu(II) ions by GGBFS and PS.

Isotherm model	Parameters	Adsorbent	
		GGBFS	PS
Langmuir	K_L (L/mg)	0.0108	0.0050
	q_m (mg/g)	156.30	151.52
	R^2	0.9951	0.9867
Freundlich	K_f ($mg^{1-n}.L^n/g$)	0.8473	0.5999
	n	0.2246	0.3068
	R^2	0.9682	0.9938

Table 5: Dimensionless separation factor of Cu(II) adsorption by PS and GGBFS.

C_0 (mmol/L)	R_L	
	PS	GGBFS
5	0.948	0.976
20	0.822	0.909
50	0.649	0.799
100	0.480	0.666
200	0.316	0.499
500	0.156	0.285
1000	0.085	0.166

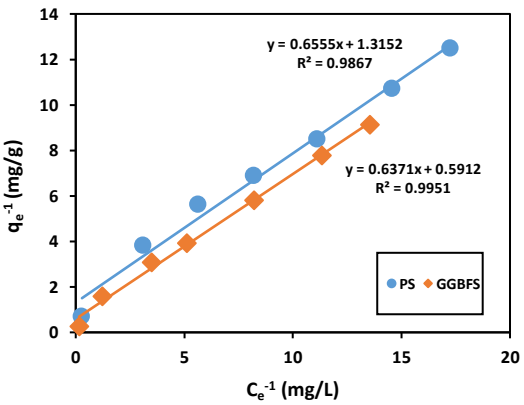

Fig. 3: The Langmuir isotherm model data of adsorption capacity for PS and GGBFS.

that the adsorption is linear, $R_L = 0$ demonstrates an irreversible process, and $0 < R_L < 1$ indicates a desirable adsorption process. By tending this value to zero, the desirability of the process is increased. Table 5 presents the R_L values for different initial concentrations of Cu(II) in the solution using both adsorbents. An increase in the initial concentration of Cu(II) higher than 1000 mmol/L causes the desirability of the adsorption process.

The adsorption capacity of GGBFS and PS for the Cu(II) adsorption was compared with the adsorption capacity of several adsorbents presented in Table 6. From the reported data, both studied adsorbents in this study have an acceptable equilibrium adsorption capacity in addition to being inexpensive and available. Therefore, these two adsorbents can be widely applied on the industrial scale.

Adsorption Thermodynamics

The experiments were carried out at 30, 45, 60, and 70°C to survey the adsorption thermodynamics for the calculation of enthalpy changes (ΔH°), entropy changes (ΔS°), and Gibbs free energy changes (ΔG°). The values of ΔH° and ΔS° are calculated by Eq. (9) [42].

$$\ln K_L = \frac{\Delta S^\circ}{R} - \frac{\Delta H^\circ}{R T} \quad (9)$$

Where K_L (L/mg) is the equilibrium constant, T (K) is absolute temperature, R (J/(mol.K)) is the general gases constant, and ΔH° (J/mol) and ΔS° (J/(mol.K)) are the enthalpy and entropy changes, respectively. As can be seen in Fig. 4, a straight line is attained by plotting $\ln(K_L)$ in $\frac{1}{T}$. The enthalpy and entropy changes are determined from the slope and the intercept of this straight line, respectively. According to the calculations, the values of enthalpy changes are -14.755 and -29.448 kJ/mol for the PS and GGBFS, respectively. Therefore, the Cu(II) adsorption is an exothermic process for both PS and GGBFS. Also, the low amount of enthalpy changes shows that the mechanism of the adsorption is physical.

Table 6: The comparison of Cu(II) maximum adsorption capacity for various adsorbents.

Adsorbent	q_m (mg/g)	Reference
Clay	12.83	[38]
Spruce wood	2.01	[39]
Pine bark	1.90	[39]
Cork	4.81	[39]
Leonardite	4.72	[39]
Bituminouc coal	1.35	[39]
Cock	3.05	[39]
Lentil shell	9.59	[40]
Wheat shell	17.42	[40]
Rice shell	2.95	[40]
Dolomite	1.63	[41]
Activated carbon (AC)	104.17	[19]
Areca Catechu stem-based AC	68.09	[20]
Nano kaolinite	125.00	[21]
Crosslinked chitosan/Waste Active Sludge Char (WASC) beads	980.80	[22]
Magnetic tubular carbon nanofibers (MTCFs)	375.93	[23]
GP-CTAB	108.20	[24]
GGBFS	156.30	Present study
PS	151.52	Present study

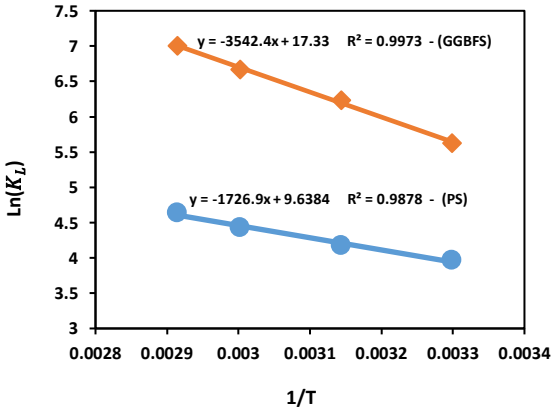

Fig. 4: Plot of ln K_L vs. 1/T for the Cu(II) adsorption using PS and GGBFS.

The values of entropy changes in the Cu(II) adsorption are 81.41 and 144.08 J/mol for the PS and GGBFS, respectively. The positive values of the entropy changes indicate that the irregularity increase in the adsorption process. This increase in irregularity can be attributed to the surface complexion. The thermodynamic parameters are reported in Table 7.

The Gibbs free energy changes are obtained using equation 10 with the values of ΔH° and ΔS° known. Gibbs free energy changes of the Cu(II) adsorption on GGBFS and PS are shown in table 7. The negativity of these values represents the self-occurrence of the adsorption process.

$$\Delta G^\circ = \Delta H^\circ - T\Delta S^\circ \quad (10)$$

Effect of initial concentration

The effects of the initial concentration of Cu(II) on the adsorption capacity and removal percentage are exhibited in Figs. 5A and B, respectively, for both adsorbents PS and GGBFS. As shown in Fig. 5A, the adsorption capacity increases by enhancing the initial concentration up to 500 mg/L, and then, the adsorption capacity remains constant at concentrations higher than 500 mg/L. According to Fig. 5B, the maximum removal capacities are 6.65 and 9.69 mg/L for the PS and GGBFS, respectively. Hence, the GGBFS is more suitable than PS for Cu(II) adsorption under the studied conditions. According to Fig. 5B in the concentration range of 5-1000 mg/L, the highest removal percentage of contamination by both adsorbents occurs at a concentration of 50 mg/L. Therefore, the initial concentration of Cu(II) was considered 50 mg/L for the following investigations.

Effect of shaking rate

The removal percentage of Cu(II) in different rotation rates is depicted in Fig. 6. As shown, the adsorption percentage increases by increasing the rotation rate from 15 to 150 rpm, while it remained constant at 97% by enhancing the rotation rate to over 150 rpm. This observation can be justified in the sense that when the rotation rate is low, the mass transfer controller stage is the transfer of Cu(II) from bulk to the adsorbent surface. In this situation, the mass transfer coefficient in bulk is increased caused by the rotation rate enhancement that led to an increase in the Cu(II) removal. However, the mass transfer controller stage is the Cu(II) adsorption

Table 7: Thermodynamic parameters of Cu(II) adsorption by PS and GGBFS.

Adsorbent	ΔH° (kJ/mol)	ΔS° (kJ/(mol. K))	ΔG° (kJ/mol)
PS	-14.755	81.410	-39.027
GGBFS	-29.448	144.080	-72.406

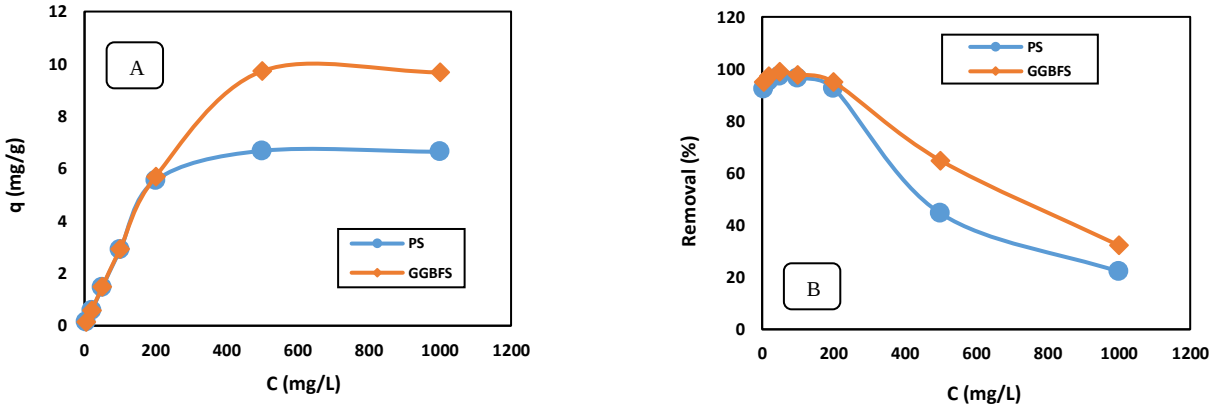

Fig. 5: Effect of initial concentration on (A) Cu(II) adsorption capacity, and (B) Cu(II) removal by PS and GGBFS.

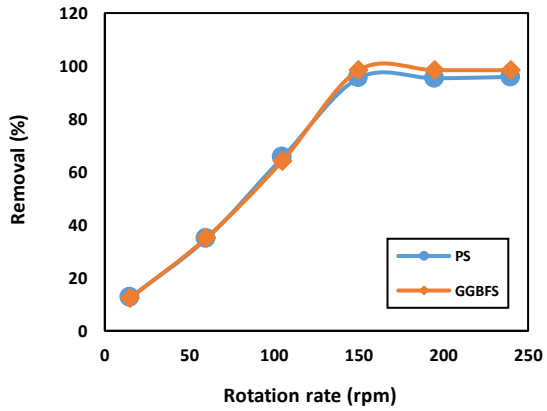

Fig. 6: Effect of rotation rate on the Cu(II) removal using PS and GGBFS.

process the adsorbent at a rate above 150 rpm, and hence, with a further increase in the rotation rate, the removal percentage of Cu(II) remains constant [35]. So, the rotation rate of 150 rpm was selected as the optimal rate. Also, based on Fig. 6, because the adsorption control stage is the transition of Cu(II) from bulk to the adsorbent surface and not the adsorption tendency to Cu(II) adsorption in the rotation rate of less than 150 rpm, the adsorption rate is approximately equal for both adsorbents. However, in rotation rate greater than 150 rpm, in which the adsorption of transferred ions from bulk to the adsorbent surface is the adsorption process controller stage, it is observed that the adsorption capacity of GGBFS is greater than PS at a constant rotation rate. It means the tendency of GGBFS for the Cu(II) removal is higher than PS due to a larger specific area of GGBFS than PS one acquired from Table 2. Therefore, the GGBFS has more active sites for Cu(II) adsorption.

Effect of adsorbent dosage

The influence of adsorbent dosage on the percentage of Cu(II) removal with an initial concentration of 50 mg/L is shown in Fig. 7. The maximum amount of GGBFS for the Cu(II) adsorption was obtained 0.2 g per 0.03 L. So that if the GGBFS weight increases to more than this optimal amount, the removal percentage remains constant at 97%. Also, the optimum PS weight for the Cu(II) adsorption was achieved 0.5 g per 0.03 L.

CONCLUSIONS

In this study, the removal of Cu(II) was investigated using GGBFS and PS as the adsorbents experimentally. The effects of operating conditions including the initial concentration of Cu(II), rotation rate, adsorbent dosage, and temperature on the adsorption capacity were examined. The optimal values of the initial concentration and rotation rate were determined to be 50 mg/L and 150 rpm,

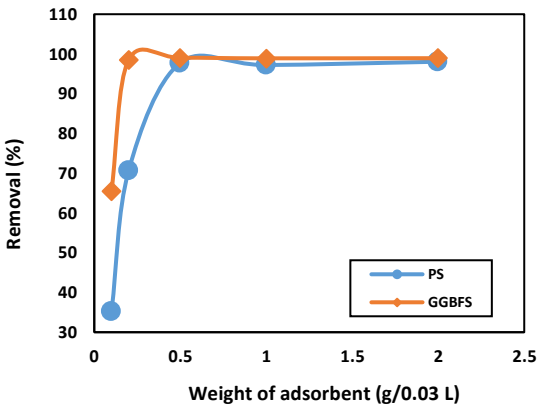

Fig. 7: Effect of the weight of adsorbents on the Cu(II) removal by PS and GGBFS.

respectively. The second-order kinetic model, as well as Freundlich and Langmuir isotherm models, confirm the experimental data of the Cu(II) adsorption process for both adsorbents. The adsorption process reaches equilibrium in less than 5 min. The adsorption capacities of Cu(II) by GGBFS and PS, which are low-cost materials produced as by-products in the industry, are more than many other natural and mineral adsorbents. According to thermodynamic studies, the Cu(II) removal process is physical adsorption. The regeneration process of these two adsorbents can be considered in future research for industrial applications.

Received : Mar. 24, 2021 ; Accepted : May 31, 2021

REFERENCES

[1] Khajeh M., Heidari Z.S., Sanchooli E. Synthesis, Characterization and Removal of Lead from Water Samples Using Lead-Ion Imprinted Polymer, *Chemical Engineering Journal*, **166(3)**: 1158-1163 (2011).

[2] Samiey B., Cheng C.-H., Wu J., Organic-Inorganic Hybrid Polymers as Adsorbents for Removal of Heavy Metal Ions from Solutions: A Review, *Materials*, **7**(2) 673-726 (2014).

[3] Muslim A., Aprilia S., Suha T., Fitri Z. Adsorption of Pb(II) Ions from Aqueous Solution Using Activated Carbon Prepared from Areca Catechu Shell: Kinetic, Isotherm and Thermodynamic Studies, *Journal of Korean Chemical Society*, **61(3)**: 89-96 (2017).

[4] Muslim A., Optimization of Pb(II) Adsorption onto Australian Pine Cones-Based Activated Carbon by Pulsed Microwave Heating Activation, *Iranian Journal of Chemistry and Chemical Engineering Journal (IJCCE)*, **36**(5) 115-127 (2017).

[5] Kalyani S., Priya J.A., Rao P.S., Krishnaiah A.J.S., Removal of Copper and Nickel From Aqueous Solutions Using Chitosan Coated on Perlite as Biosorbent, *Separation Science and Technology*, **40(7)**: 1483-1495 (2005).

[6] Hasan S., Krishnaiah A., Ghosh T.K., Viswanath D.S., Boddu V.M., Smith E. D., Adsorption of Divalent Cadmium (Cd (II)) from Aqueous Solutions onto Chitosan-Coated Perlite Beads, *Industrial & Engineering Chemistry Research*, **45(14)**:5066-5077 (2006).

[7] Gier S., Johns W.D., Heavy Metal-Adsorption on Micas and Clay Minerals Studied by X-Ray Photoelectron Spectroscopy, *Applied Clay Science*, **16(5-6)**: 289-299 (2000).

[8] Koppelman M., Dillard J. A Study of the Adsorption of Ni (II) and Cu (II) by Clay Minerals, *Clays & Clay Minerals*, **25(6)**: 457-462 (1977).

[9] Ghaemi A., Torab-Mostaedi M., Ghannadi-Maragheh M., Characterizations of Strontium (II) and Barium (II) Adsorption from Aqueous Solutions Using Dolomite Powder, *Journal of Hazardous Materials*, **190(1-3)**: 916-921 (2011).

[10] Rahmati A., Ghaemi A., Samadfam M., Kinetic and Thermodynamic Studies of Uranium (VI) Adsorption Using Amberlite IRA-910 Resin, *Annals of Nuclear Energy*, **39(1)**: 42-48 (2012).

[11] Mohammadi M., Ghaemi A., Torab-Mostaedi M., Asadollahzadeh M., Hemmati A., Adsorption of Cadmium (II) and Nickel (II) on Dolomite Powder, *Desalination & Water Treatment*, **53(1)**: 149-157 (2015).

[12] Huang S.-H., Chen D.-H., Rapid Removal of Heavy Metal Cations and Anions From Aqueous Solutions by an Amino-Functionalized Magnetic Nano-Adsorbent, *Journal of Hazardous Materials*, **163(1)**: 174-179 (2009).

[13] Sun X., Yang L., Li Q., Zhao J., Li X., Wang X., Liu H., Amino-Functionalized Magnetic Cellulose Nanocomposite as Adsorbent for Removal of Cr (VI): Synthesis and Adsorption Studies, *Chemical Engineering Journal*, **241**: 175-183 (2014).

[14] Tan Y., Chen M., Hao Y., High Efficient Removal of Pb (II) by Amino-Functionalized Fe_3O_4 Magnetic Nano-Particles, *Chemical Engineering Journal*, **191**: 104-111 (2012).

[15] Han R., Zhang J., Zou W., Xiao H., Shi J., Liu H., Biosorption of Copper (II) and Lead (II) from Aqueous Solution by Chaff in a Fixed-Bed Column, *Journal of Hazardous Materials*, **133(1-3)**: 262-268 (2006).

[16] Fu F., Wang Q., Removal of Heavy Metal Ions from Wastewaters: A Review, *Journal of Environmental Management*, **92(3)**: 407-418 (2011).

[17] Tizaoui C., Rachmawati S.D., Hilal N., The Removal of Copper in Water Using Manganese Activated Saturated and Unsaturated Sand Filters, *Chemical Engineering Journal*, **209**: 334-344 (2012).

[18] Ahmaruzzaman M., Industrial Wastes as Low-Cost Potential Adsorbents for the Treatment of Wastewater Laden with Heavy Metals, *Advances in Colloid and Interface Science*, **166(1-2)**: 36-59 (2011).

[19] Muslim A., Ellysa E., Said S.D., Cu (II) Ions Adsorption Using Activated Carbon Prepared from Pithecellobium Jiringa (Jengkol) Shells with Ultrasonic Assistance: Isotherm, Kinetic and Thermodynamic Studies, *Journal of Engineering and Technological Sciences*, **49(4):** 472-490 (2017).

[20] Muslim A., Marwan, M., Saifullah, R., Azwar, M., Darmadi, D., Putra, B.P., Rizal, S., Adsorption of Cu(II) Ions on Areca Catechu Stem-Based Activated Carbon: Optimization Using Response Surface Methodology, *International Review on Modelling and Simulations (IREMOS),* "Adsorption; Activated Carbon; Areca Catechu Stem; Modeling; Optimization; Box Benkhen" **12(2)** (2019).

[21] Alasadi A., Khaili F., Awwad A., Adsorption of Cu (II), Ni (II) and Zn (II) Ions by Nano Kaolinite: Thermodynamics and Kinetics Studies, *Chemistry International*, **5(4)**: 258-226 (2019).

[22] Dandil S., Sahbaz D.A., Acikgoz C., Adsorption of Cu (II) Ions onto Crosslinked Chitosan/Waste Active Sludge Char (WASC) Beads: Kinetic, Equilibrium, and Thermodynamic Study, *International Journal of Biological Macromolecules*, **136**: 668-675 (2019).

[23] Ahmad M., Wang J., Xu J., Zhang Q., Zhang B., Magnetic Tubular Carbon Nanofibers as Efficient Cu (II) Ion Adsorbent from Wastewater, *Journal of Cleaner Production*, **252**: 119825 (2020).

[24] Yu Z., Song W., Li J., Li Q., Improved Simultaneous Adsorption of Cu(II) and Cr(VI) of Organic Modified Metakaolin-Based Geopolymer, *Arabian Journal of Chemistry*, (2020).

[25] Guo X., Zhang S., Shan X., Adsorption of Metal Ions on Lignin, *Journal of Hazardous Materials*, **151(1)**: 134-142 (2008).

[26] Shi K., Wang X., Guo Z., Wang S., Wu W., Se(IV) Sorption on TiO_2: Sorption Kinetics and Surface Complexation Modeling, *Colloids and Surfaces A: Physicochemical and Engineering Aspects*, **349(1-3)**: 90-95 (2009).

[27] Korichi S., Bensmaili A., Sorption of Uranium (VI) on Homoionic Sodium Smectite Experimental Study and Surface Complexation Modeling, *Journal of Hazardous Materials*, **169**(1-3): 780-793 (2009).

[28] Maghsoodloorad H., Allahverdi A., Alkali-Activation Kinetics of Phosphorus Slag Cement Using Compressive Strength Data, *Ceramics–Silikáty*, **59(3)**: 250-260 (2015).

[29] Zaki M.I., Hasan M.A., Al-Sagheer F.A., Pasupulety L., In Situ FTIR Spectra of Pyridine Adsorbed on SiO_2–Al_2O_3, TiO_2, ZrO_2 and CeO_2: General Considerations for the Identification of Acid Sites on Surfaces of Finely Divided Metal Oxides, *Colloids and Surfaces A: Physicochemical and Engineering Aspects*, **190**(3): 261-274 (2001).

[30] Lagergren S., Lagergren S., Lagergren S., Sven K., "Zurtheorie Der Sogenannten Adsorption Gelösterstoffe" (1898).

[31] Ho Y.-S., McKay G., Pseudo-Second order Model for Sorption Processes, *Process Biochemistry*, **34(5)**: 451-465, (1999).

[32] Freundlich H., Over the Adsorption in Solution, *J. Phys. Chem*, **57(385471)**: 1100-1107, (1906).

[33] Adamson A. W., Gast A.P., "Physical Chemistry of Surfaces". Interscience Publishers, New York, (1967).

[34] Kundu S., Gupta A., Arsenic Adsorption onto Iron Oxide-Coated Cement (IOCC): Regression Analysis of Equilibrium Data with Several Isotherm Models and Their Optimization, *Chemical Engineering Journal*, **122(1-2)**: 93-106 (2006).

[35] Pérez-Marín A., Zapata V.M., Ortuno J., Aguilar M., Sáez J., Lloréns M., Removal of Cadmium from Aqueous Solutions by Adsorption onto Orange Waste, *Journal of Hazardous Materials*, **139(1)**: 122-131 (2007).

[36] Langmuir I., The Constitution and Fundamental Properties of Solids and Liquids. Part I. Solids, *Journal of the American Chemical Society*, **38(11)**: 2221-2295 (1916).

[37] Weber T.W., Chakravorti R.K., Pore and Solid Diffusion Models for Fixed-Bed Adsorbers, *AIChE Journal*, **20(2)**: 228-238 (1974).

[38] Khazali O., Abu-El-Halawa R., Al-Sou'od K. Removal of Copper (II) from Aqueous Solution by Jordanian Pottery Materials, *Journal of Hazardous Materials*, **139(1)**: 67-71 (2007).

[39] Hanzlik P., Jehlicka J., Weishauptova Z., Sebek O., Adsorption of Copper, Cadmium and Silver from Aqueous Solutions onto Natural Carbonaceous Materials, *Plant Soil and Environment*, **50(6)**: 257-264 (2004).

[40] Aydın H., Bulut Y., Yerlikaya Ç., Removal of Copper (II) From Aqueous Solution by Adsorption onto Low-Cost Adsorbents, *Journal of Environmental Management*, **87(1)**: 37-45 (2008).

[41] Ghaemi A., Torab-Mostaedi M., Shahhosseini S., Asadollahzadeh M., Characterization of Ag (I), Co (II) and Cu (II) Removal Process from Aqueous Solutions Using Dolomite Powder, *Korean Journal of Chemical Engineering*, **30(1)**: 172-180 (2013).

[42] Li Y.-H., Di Z., Ding J., Wu D., Luan Z., Zhu Y., Adsorption Thermodynamic, Kinetic and Desorption Studies of Pb^{2+} on Carbon Nanotubes, *Water Research*, **39(4)**: 605-609 (2005).